

Organic & Biomolecular Chemistry

Accepted Manuscript

This article can be cited before page numbers have been issued, to do this please use: P. Jana, A. Siva, V. Soppina and S. Kanvah, *Org. Biomol. Chem.*, 2020, DOI: 10.1039/D0OB01277G.



This is an Accepted Manuscript, which has been through the Royal Society of Chemistry peer review process and has been accepted for publication.

Accepted Manuscripts are published online shortly after acceptance, before technical editing, formatting and proof reading. Using this free service, authors can make their results available to the community, in citable form, before we publish the edited article. We will replace this Accepted Manuscript with the edited and formatted Advance Article as soon as it is available.

You can find more information about Accepted Manuscripts in the [Information for Authors](#).

Please note that technical editing may introduce minor changes to the text and/or graphics, which may alter content. The journal's standard [Terms & Conditions](#) and the [Ethical guidelines](#) still apply. In no event shall the Royal Society of Chemistry be held responsible for any errors or omissions in this Accepted Manuscript or any consequences arising from the use of any information it contains.

Live-cell Imaging of Lipid Droplets by Solvatochromic Coumarin Derivatives

View Article Online
DOI: 10.1039/D0OB01277GPalash Jana[#], Aravintha Siva[†], Virupakshi Soppina^{†*} and Sriram Kanvah^{**}

[#]Department of Chemistry, Indian Institute of Technology Gandhinagar,
Palaj, Gandhinagar 382355, India.

e-mail: sriram@iitgn.ac.in, kanvah@gatech.edu

[†]Department of Biological Engineering, Indian Institute of Technology Gandhinagar
Palaj Gandhinagar 382355

e-mail: vsoppina@iitgn.ac.in, vsoppina@gmail.com

Abstract

Lipid droplets (LDs), the lipid-rich intracellular organelles, serve to regulate many physiological processes and therefore attracted attention towards selective detection of lipid droplets. We report positively solvatochromic lipophilic dyes, based on the push-pull framework containing coumarin-pyridine heterocycles for selective live-cell imaging of lipid droplets (LDs) in Cos-7 and McA-RH7777 cells at ultralow concentrations (200 nM). The fluorescence probes show a remarkable increase in fluorescence intensity with time with the hydrophobic core of the lipid droplets contributing to the observed intensity enhancement. The simple structural framework, red-emission, strong Stokes shift (>80 nm), excellent biocompatibility highlights their significance as a versatile imaging tool for studying of Lipid droplets (LDs).

Introduction

Lipid droplets (LDs) are specialized intracellular organelles in cells and organisms, which evolved as a universal energy reservoir mechanism in both eukaryotes and prokaryotes¹⁻⁵. These ubiquitous organelles are composed of a phospholipid monolayer that encapsulates triglycerols and sterol esters. A plethora of proteins decorates the surface of these organelles, including the membrane protein perilipin, membrane trafficking proteins like Rab5 and Rab18, and enzymes such as triglycerol lipases that are involved in lipid metabolism⁶⁻⁹. Although different models postulate different mechanisms of lipid droplet formation, the common belief is that these organelles originate from the endoplasmic reticulum¹⁰. LDs play essential roles in several cellular processes that include the production of energy, formation of membranes, carriers of lipids, protein-protein interactions, and metabolism of fats^{5, 11}. Besides, they also

play crucial roles in other cellular processes including lipid ligand generation and transcription factor sequestration¹². The dynamics and functions of these droplets are further complicated by their interaction with multiple other organelles like the mitochondria, endosomes, and endoplasmic reticulum¹³. Due to their critical role in numerous such cellular events, any abnormalities in these organelles are implicated in the development of metabolic diseases. Multiple reports state the involvement of these organelles in health conditions such as obesity, diabetes, atherosclerosis, neurodegeneration, and fatty liver diseases^{12, 14, 15}. Despite the vast influx of information on the importance of these dynamic structures in the recent past, fundamental questions on the composition, function, and biogenesis of these organelles remain mostly unanswered.

This shortage of information is partially attributed to the lack of techniques that help us visualize these structures inside the cell. While conventional microscopic methods like light microscopy do contribute to the study of the biophysical properties of these organelles, they usually require the cells to be fixed and processed. On the other hand, imaging of these organelles with fluorescent dyes aids significantly in understanding their dynamics and localization in live-cell conditions^{16, 17}. Therefore, to visualize real-time and get insights on their interactions, highly sensitive fluorescence microscopy-based imaging tools were much sought¹⁸. The use of organelle-specific fluorophores will allow the study of precise localization and dynamics of different sub-cellular components. In particular, the use of donor or acceptor substituted fluorophores have attracted significant attention owing to their potential applicability for sensing and bioimaging¹⁹⁻²². The research on lipid droplets gained momentum with the simultaneous synthesis of a variety of fluorescent dyes, including Nile Red²³, Bodipy^{24, 25}, cyanine dyes¹⁷, Lipid Green²⁶, push-pull²⁷⁻³⁰ and amphipathic derivatives^{31, 32}, and others^{33, 34}. Some limitations of the dyes include narrower Stokes shift, photostability, complicated or expensive synthetic strategies, interfering background signals and low specificity in live cells. Dyes such as Oil Red O and Sudan III also suffer from such drawbacks in addition to being disruptive to the cells in a few cases, resulting in false-positive observations. Despite the rapid development of organic fluorophores, newer molecules are continually being developed for stronger and selective imaging of the lipid droplets. A summary of some recent imaging lipid droplets using organic fluorophores is shown in table S1.

View Article Online
DOI: 10.1039/C9OB01277G

In this report, we propose a simple coumarin-substituted styrylpyridines as potential molecules for imaging lipid droplets [Fig-1]. Both coumarin and pyridine moieties are extensively used for biological applications and form a crucial structural component of many natural product scaffolds. The presence of diethylamino or julolidine electron donating groups helps in shifting the intramolecular charge transfer bands to the red-wavelength regions. Further, the donor-acceptor structural framework separated by the styryl bridge also yields a relatively significant Stokes shift. Moreover, suitably substituted coumarin derivatives are also used as excellent fluorescent reporters³⁵⁻³⁹. In the present report, we synthesized and characterized two simple styrylcoumarin probes and demonstrated the tracking of lipid droplets inside the cell and the study enables future investigations in understanding the dynamics of these organelles and studying disease models.

Experimental

The chemicals required for the synthesis of pyridine acrylonitrile derivatives were obtained from Aldrich, Alfa Aesar, Sigma-Aldrich, and S. D. Fine. The UV-Vis absorption spectral data were measured using Analytic Jena, Specord 210 spectrophotometer. The emission spectra were recorded using the Horiba Fluorolog-3 spectrofluorimeter. The synthesized samples were characterized using NMR and HRMS obtained using Bruker Avance 500 MHz NMR spectrometer and Waters-Synapt G2S (ESI-QToF) mass spectrometer, respectively. For the absorption or fluorescence studies, 10 μL of the desired fluorophore-stock solution in dioxane ($\sim 10^{-3}$ M) was added to 1 mL (effective concentration ~ 10 μM) of the desired solvent media, and the samples were excited at their respective absorption maxima (λ_{abs}).

Reagents and plasmids

All reagents for molecular biology, cell culture, and imaging experiments were purchased from Sigma-Aldrich, Thermofisher Scientific, and New England Bio Labs (NEB) unless otherwise mentioned. HPos is a peptide that is putatively used as a lipid droplet-targeting sequence. The plasmid DNA for HPos and the commercial lipid droplet stain, Oil Red O were a kind gift from Prof. Roop Mallik, TIFR, Mumbai. We generated the HPos-mCherry plasmid by sub-cloning the HPos using appropriate restriction sites into mCherry-N1 backbone plasmid. All the plasmids used in the study were verified by DNA sequencing.

Cell culture and transfection

View Article Online
DOI: 10.1039/D0OB01277G

Cervical adenocarcinoma (HeLa), COS-7 (monkey kidney fibroblast, ATCC), and rat liver cells (McA-RH7777) cells were grown in DMEM supplemented with 10% fetal bovine serum (FBS) and 2 mM L-glutamine at 37 °C with 5% CO₂. Cells were transfected with 1.0 µg of plasmid DNA using Lipofectamine-3000 transfection reagent.

MTT assays

For MTT, five thousand HeLa cells were seeded (per well) in a 96-well plate. These cells were subsequently treated with varying concentrations of the probes for 24 h following which, they were incubated with MTT for 4 h. DMSO was then added to solubilize the formazan, and the absorbance was recorded at 570 nm using BioTek SYNERGYH1 plate reader.

Fluorescence Live-cell imaging

For live-cell studies, 0.1 million Cos-7/McA-RH7777 cells were seeded on 35 mm glass-bottom plates. The cells were treated with 200 nM of the respective probes (**J-1** and **C-1**) for 10 and 30 minutes, respectively. The plates were then washed thrice with Fluorobrite imaging medium and images were obtained on an inverted epifluorescence Nikon Ti2 Eclipse microscope, equipped with 60X 1.49 NA objective and an EMCCD camera (Andor iXon 897Ultra, Andore Technologies, USA). The images were acquired at a speed of 10 fps and stored in the form of movies. For co-distribution studies with Oil Red O, 0.1 million Cos-7 cells were seeded on 35 mm glass-bottom plates. Cells were first incubated with Oil Red O and images were captured in the red channel. Following this, the cells were incubated with 200 nM of the respective probes (**C-1** and **J-1**) and images were taken in green channel.

Data analysis

The image analysis and quantification were performed using ImageJ software (nih.gov). Cells were randomly selected to perform the quantification. The value of maximum fluorescence intensity was obtained from ImageJ. Background fluorescence was subtracted from this maximum value to get the fold change in intensity.

Results and Discussion

Synthesis of fluorophores 1 and 2

Two fluorescent probes bearing coumarin and pyridine scaffolds (C-1 and J-1) were synthesized by a condensation reaction of pyridine acrylonitrile with the corresponding aldehyde **4** & **7** (Fig-1). The aldehydes (**4** and **7**) used were synthesized by following published literature^{35, 40}. The aldehydes **2** and **5** were cyclized with malonic ester in the presence of piperidine to achieve coumarin scaffold **3** and **6** with diethylamine and julolidine donating groups respectively. Vilsmeier-Haack formylation of **3** and **6** yields the desired aldehydes **4** and **7**. All the structures have been characterized using ¹H-NMR, ¹³C-NMR & HRMS. The synthesized derivatives differ with each other: a diethylamine donor in C-1 and a julolidine group in J-1. A cyanovinyl π -spacer separates both the coumarin and pyridyl group.

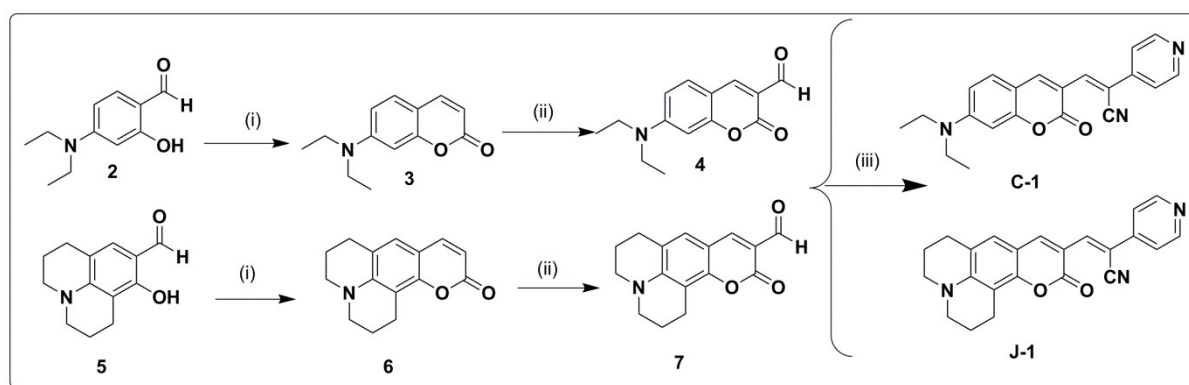


Fig 1: Synthesis of coumarin styrylpyridine probes C-1 and J-1. (i) $\text{CH}_2(\text{COOEt})_2$, Piperidine, ethanol, reflux; (ii) POCl_3 , DMF, 60°C , 8h; (iii) 4-pyridine acrylonitrile, piperidine, ethanol, reflux, 8h.

Photophysical characterization

The synthesized compounds were investigated for their optical properties in various organic solvents & water. C-1 contains a diethylamine donor while J-1 has julolidine electron donating group. The presence of julolidine may help in improve the electron-donating ability and improving the ICT absorption and emission. The compounds absorb strongly in the visible region with C-1 absorbing in the range of 477 nm-488 nm and J-1 absorbing at 498 nm. The higher absorption maxima are due to increased electron-donating ability of the julolidine moiety [Fig-2]. Moderate bathochromic absorption shifts (~ 10 nm) were noted with an increase in solvent polarity and attributed to solute-solvent interactions and energy level stabilization. Broad emission is recorded in water due to its weaker solubility and may also be due to the

formation of aggregates^{41, 42}. The emission maxima show bathochromic shifts with an increase in solvent polarity. C-1 emits at 545nm in dioxane with a change of + ~35 nm upon increasing the solvent polarity (Fig-3 & Table-1). The stronger electron-donating amino group in J-1 yields slightly larger shifts (39 nm) in the emission wavelength. The compounds are also characterized by as substantial Stokes shift 95 nm for C-1 and 93 nm in J-1.

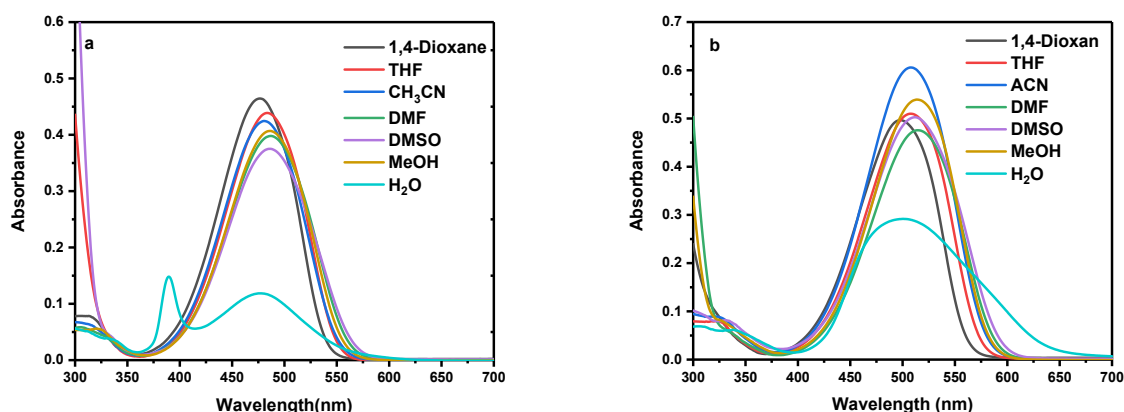


Fig 2: Absorption of a) C-1 and b) J-1 in different organic solvents

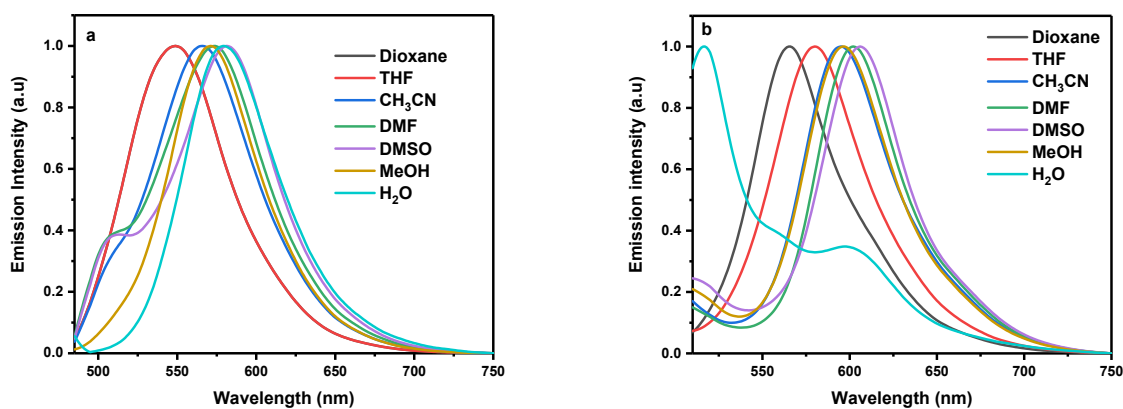


Fig 3: Emission of C-1 and J-1 in different organic solvents.

Table-1 Absorption & emission maxima of C-1 & J-1.

View Article Online
DOI: 10.1039/D0OB01277G

Solvents	C-1				J-1			
	λ_{ab} (nm)	λ_{em} (nm)	Stokes Shift (nm)	ϕ_f	λ_{ab} (nm)	λ_{em} (nm)	Stokes Shift (cm^{-1})	ϕ_f
Dioxane	477	545	68	0.059	499	564	65	0.015
THF	484	548	64	0.051	508	580	72	0.015
CH ₃ CN	481	566	85	0.043	509	595	86	0.014
DMF	488	574	86	0.038	515	601	86	0.017
DMSO	485	580	95	0.043	512	605	93	0.021
H ₂ O	478	580	102	0.012	502	599	97	0.010

ϕ_f was calculated using 0.1 M fluorescein and excited at 470 nm

Effect of Viscosity

The donor-acceptor molecular systems exhibiting strong emission due to intramolecular charge transfer have been used to study the impact of viscosity. Of particular relevance to the paper is to correlate the viscosity effects towards the localization in lipid droplets, for LDs provide hydrophobic and viscous environment compared to that of other cellular organelles. We, therefore, correlated the emission intensity of the probe with the change in viscosity of the solution. The viscosity of LDs (~ 50 cP) is significantly higher than that of cytosol (~ 1 cP)⁴³ and an increase in viscosity is expected to decrease the non-radiative transition yielding significant emission enhancement. We thus studied the emission changes of the fluorophores C-1 and J-1 in a methanol-glycerol binary mixture [Fig-4]. With increased glycerol fractions, the molecular motions are hindered yielding gradual emission intensity increments. C-1 shows a ~ 11 folds intensity increment while J-1 shows a ~ 7 folds rise in intensity along with a ~ 20 nm bathochromic emission shift. Distinct color changes also accompany the enhancement in strength. The titration of fluorophores with different surfactant (CTAB) concentrations show strong intensity enhancement with changes in micelle concentration indicating the preference to interact with viscous environment [Fig S1].

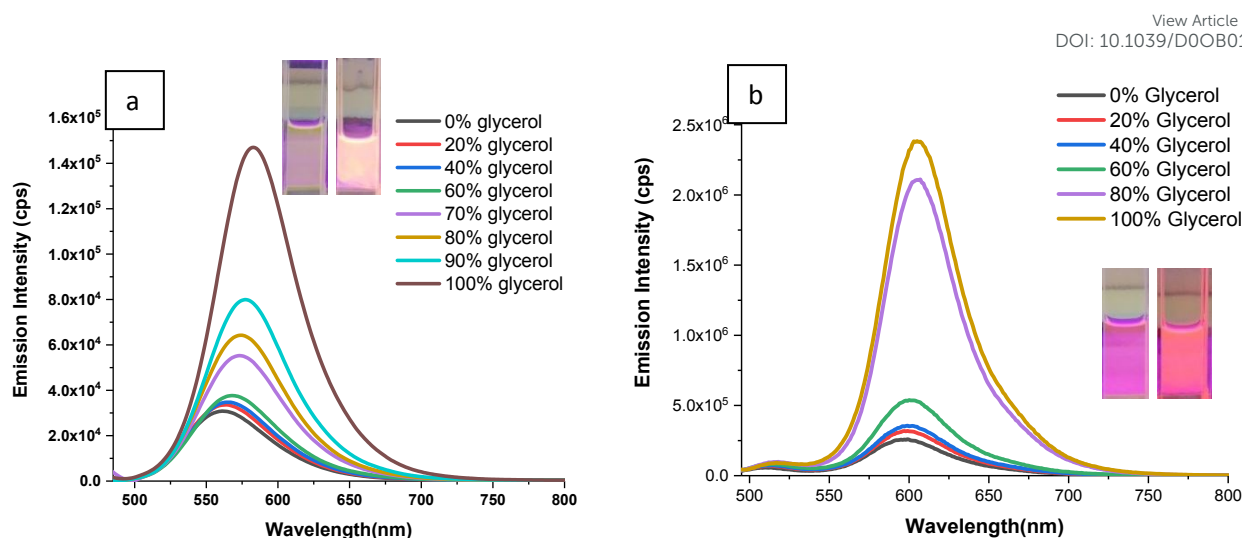


Fig-4: Increase in viscosity yields vigorous intensity and color changes: Emission of a) C-1 and b) J-1 in methanol-glycerol binary mixtures.

Effect of pH:

Considering the presence of favorable lone pair of electrons on the pyridine nitrogen and their role in controlling the photophysical properties, we studied the pH effect on C-1 and J-1. The protonation of nitrogen is expected to significantly alter the charge transfer properties. Subsequently as shown in Fig 5, increasing acidity leads to protonation of pyridine nitrogen yielding pyridinium ion that acts as strong acceptor shifting the absorption maximum to ~ 550 nm for C-1 and 585 nm in J-1 associated with strong color changes. The emission spectra shown in Fig S2 indicate shifting of the emission band to ~ 635 nm (C-1) in strongly acidic conditions associated with emission quenching for both molecules (Fig S2). This loss of emission in acidic media is attributed to formation of twisted intramolecular charge transfer excited state disturbing the planar delocalization⁴⁴.

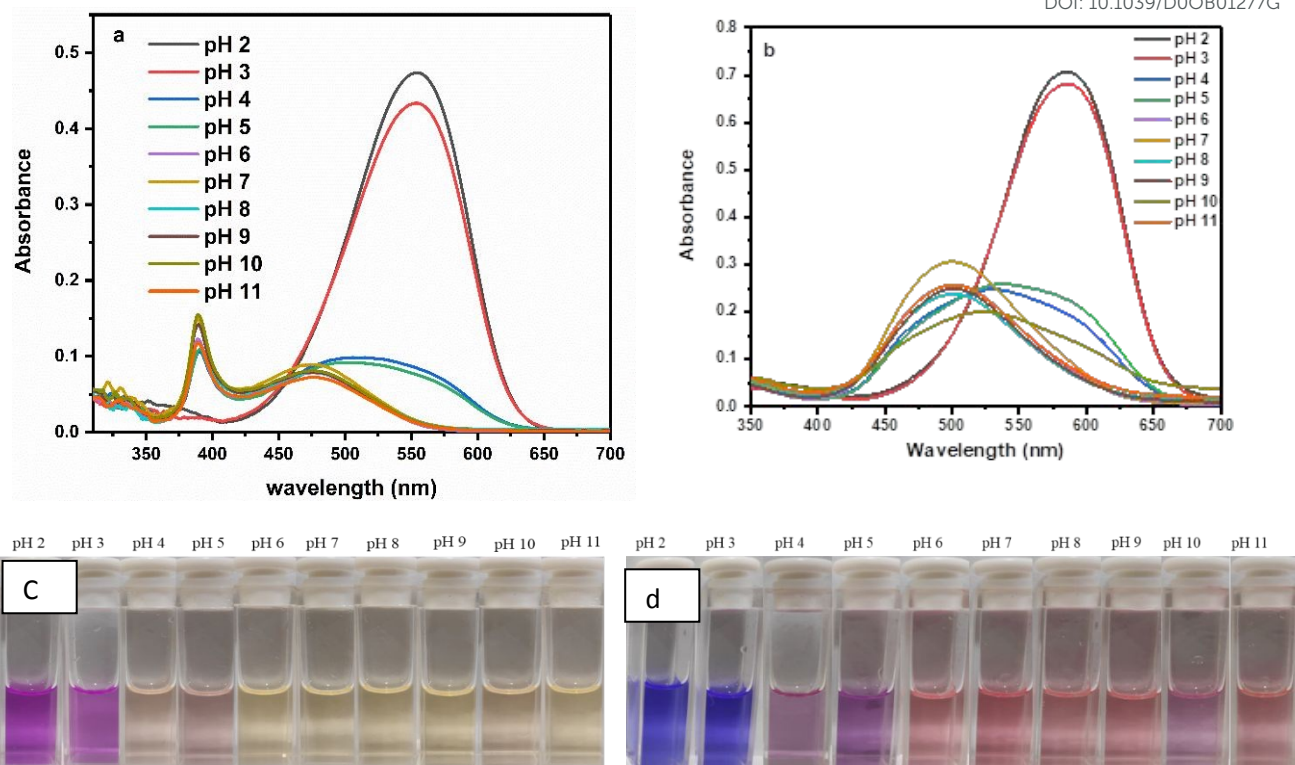


Fig 5. Absorption of C-1 and J-1 at different pH conditions. Associated color changes are shown in Fig 5c (C-1) and 5d (J-1). Fig S2 gives emission spectra

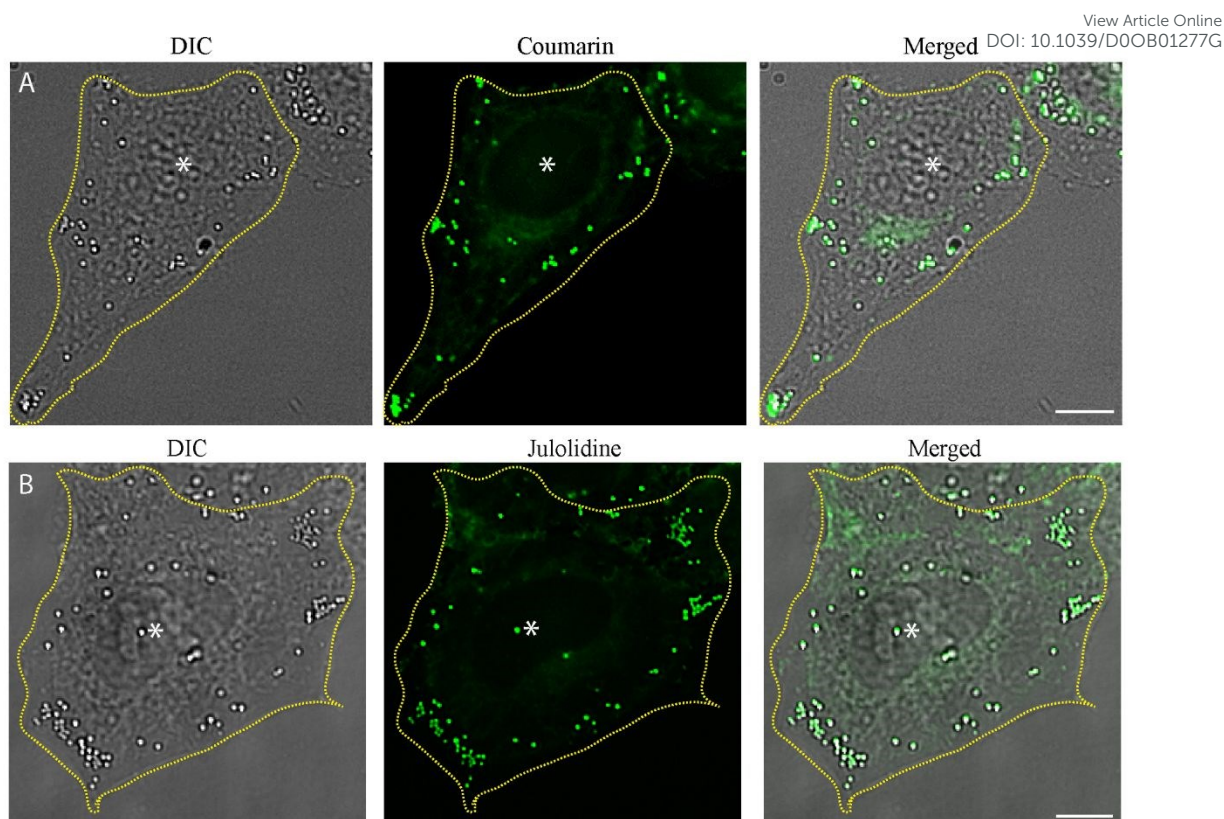


Fig 6: Probes efficiently label lipid droplets: Cos-7 cells incubated with 200 nM of A) C-1 for 30 minutes and B) J-1 for 10 minutes respectively. The highly refractile spherical structures under DIC illumination (Left panels) and fluorescently labelled bright lipid droplets (Middle panels) showed significant overlapping (Right panels) when imaged in Cos-7 cells. Scale bar represents 10 μm .

Coumarin-based probes for live-cell lipid droplet imaging.

Considering the solvatochromic emission and enhanced intensity of the fluorophores in the viscous solvents, we examined the fluorescent-tagging of lipid droplets (LDs). Cos-7 cells incubated with these fluorescent dyes (C-1 and J-1) rapidly crossed the cell membrane and showed distinct bright uniform round punctate localization distributed throughout the cytoplasm (Figure-6). Interestingly, when these cells were imaged under differential interference contrast (DIC) illumination, the above bright fluorescent punctate structures showed significant overlapping with spherical, highly refractile vesicle structures in the cytoplasm resembling lipid droplets (Fig-6). Lipid droplets, due to their considerable light diffraction properties appear as highly refractile particles under differential interference contrast (DIC) microscopy^{45, 46}. To further confirm the identity of these refractile particles, we transiently transfected cells with a plasmid coding for C-terminal mCherry-tagged HPos

(HPos-mCherry), a marker for nascent lipid droplets⁴⁷. As expected, the bright refractile particles showed a significant overlap with lipid droplets that are fluorescently labelled with HPos-mCherry (Fig. 7A). In addition, we also performed co-distribution experiments of these probes with the well-known lipid droplet stain Oil Red (Fig. 7B & C)⁴⁸. Together, our results from the co-localization studies indicate that both the probes selectively localize to and stain the lipid droplets (PCC for C-1: 0.97 ± 0.01 ; PCC for J-1: 0.96 ± 0.02) with a sizeable signal-to-noise ratio (Fig 7B & C). Moreover, such localization signals were observed even in cells treated with as low as 200 nM concentrations of the probes for the durations as short as 10 minutes.

Furthermore, to potentiate the use of these fluorescent probes across the cell types, we imaged lipid droplets in liver cancer cells. The liver is a crucial organ that functions as a part of different physiological processes, including digestion, metabolism and hormone production. Also, the liver is the main storage and metabolic center for the lipids and hence the lipid droplet levels are strictly regulated in the hepatocytes^{49, 50}. Therefore it would be exciting and clinically relevant to know whether these fluorescent probes can be used to image the lipid droplets in the hepatocytes. To test this, we incubated McA-RH7777, rat hepatoma cells with the above fluorescent probes and imaged under epifluorescence and DIC illumination. Similar to the Cos-7 cells, both the fluorophores showed distinct fluorescently labelled bright punctate localization distributed in the cytoplasm of McA-RH7777 cells that were highly refractile and spherical under DIC illumination (Figure- 8A & B), consistent with previous work⁴⁵. Together, the data suggest that the probes J-1 and C-1 have great specificity for the lipid droplets due to the strong hydrophobic core of the lipid droplets and stain the lipid droplets with the large signal-to-noise ratio. These results show good promise in extrapolating the use of these probes to clinical research.

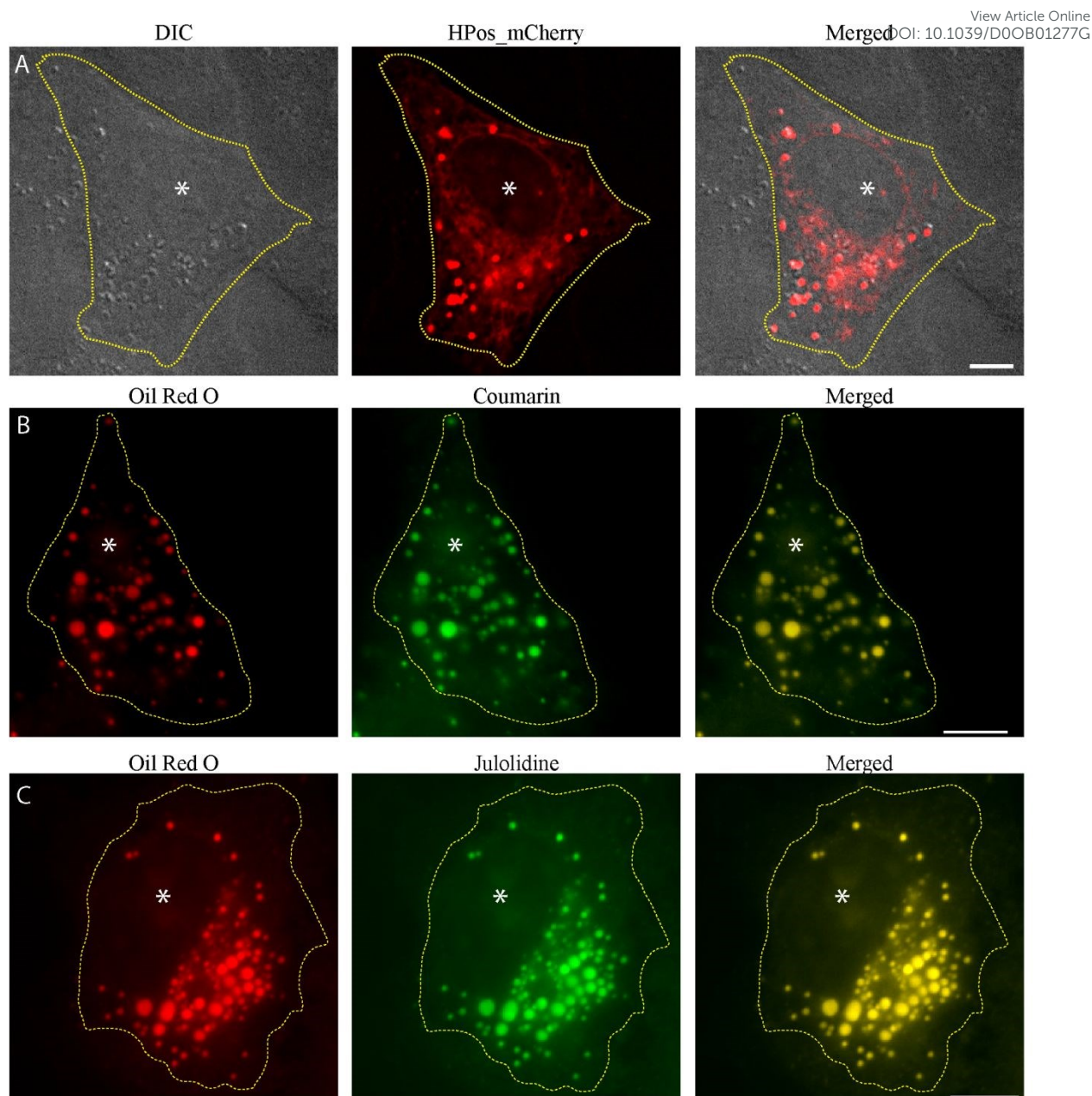


Fig 7: Probes efficiently colocalize with known lipid droplet markers: A) Cos-7 cells transfected with HPos-mCherry. Lipid droplets stained with Oil Red O (B& C: Left panels) and 200 nM of B) C-1 or C) J-1 respectively (Middle panels) showed significant overlapping (Right panels) in Cos-7 cells. (PCC for C-1: 0.97 ± 0.01 ; PCC for J-1: 0.96 ± 0.02) Scale bar represents 10 μm .

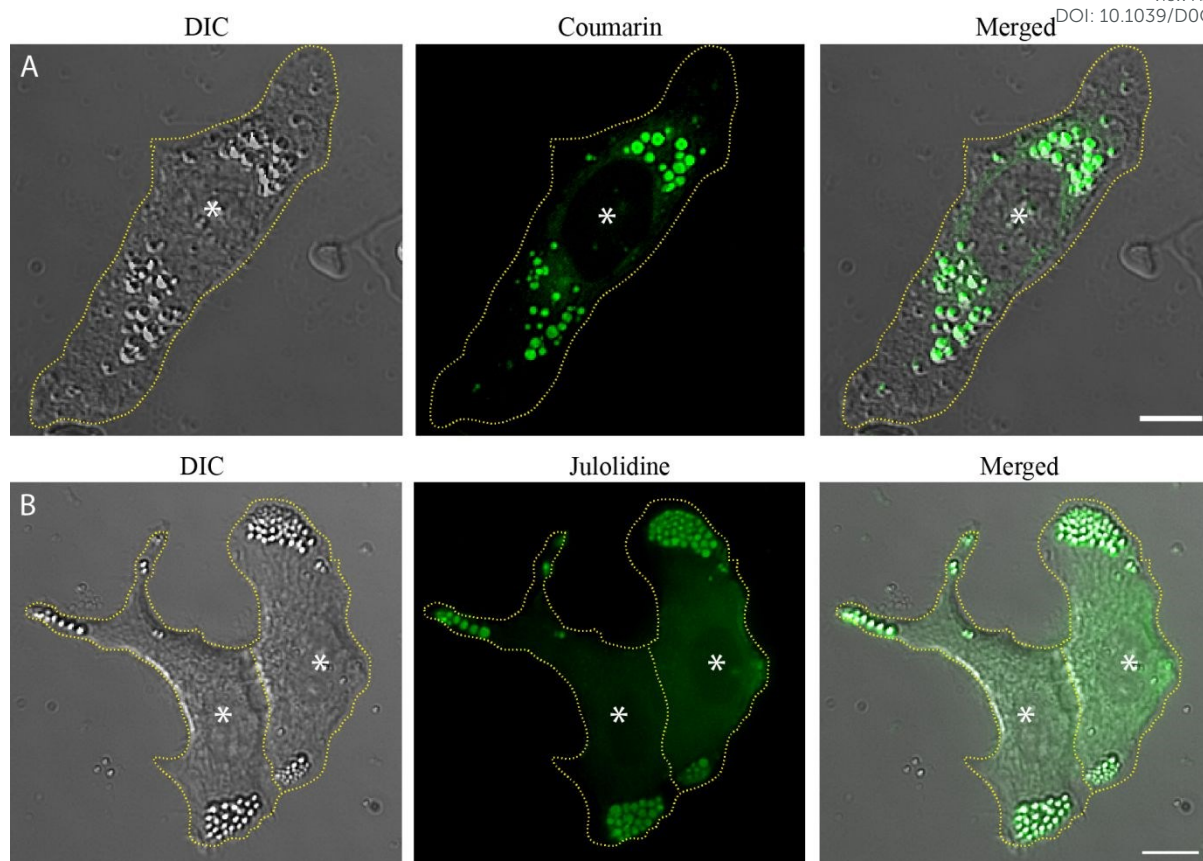


Fig 8: Probes efficiently label lipid droplets: McA-RH7777 cells incubated with 200 nM of A) C-1 and B) J-1, respectively. The highly refractile spherical structures under DIC illumination (Left panels) and fluorescently labelled bright lipid droplets (Middle panels) showed significant overlapping (Right panels) when imaged in McA-RH7777 cells. Scale bar represents 10 μm .

Novel increase in the fluorescent intensity of probes under progressive excitation

Lipid droplets are highly dynamic structures that undergo constant restructuring⁵¹. This raises the fundamental need for any fluorophore to be able to capture the dynamics of these molecules at the cellular timescale. Having known that our probes could stain the lipid droplets, we performed live-cell imaging to find out whether they were capable enough to track the dynamics of these structures for longer time-scale. Our results from real-time tracking studies of these probes showed the rapid movement and dynamics of the lipid droplets at sub-second timescales [Video 1 (C1) and Video-2 (J1): Supporting Information]. Surprisingly, unlike the conventional fluorophores that photobleach progressively upon continuous excitation, our coumarin-based probes do not photobleach over time. Instead, the fluorescent probes showed an increase in their intensity with time under constant excitation. To quantitatively analyse the progressive increase in the intensity, we recorded the fluorescent intensities of individual lipid

droplets frame-by-frame and measured the percentage change in their fluorescence intensity. Surprisingly, we observed that there was a significant increase ($P < 0.0001$; t -test) in the fluorescence signal with time (Figure- 9A & B).

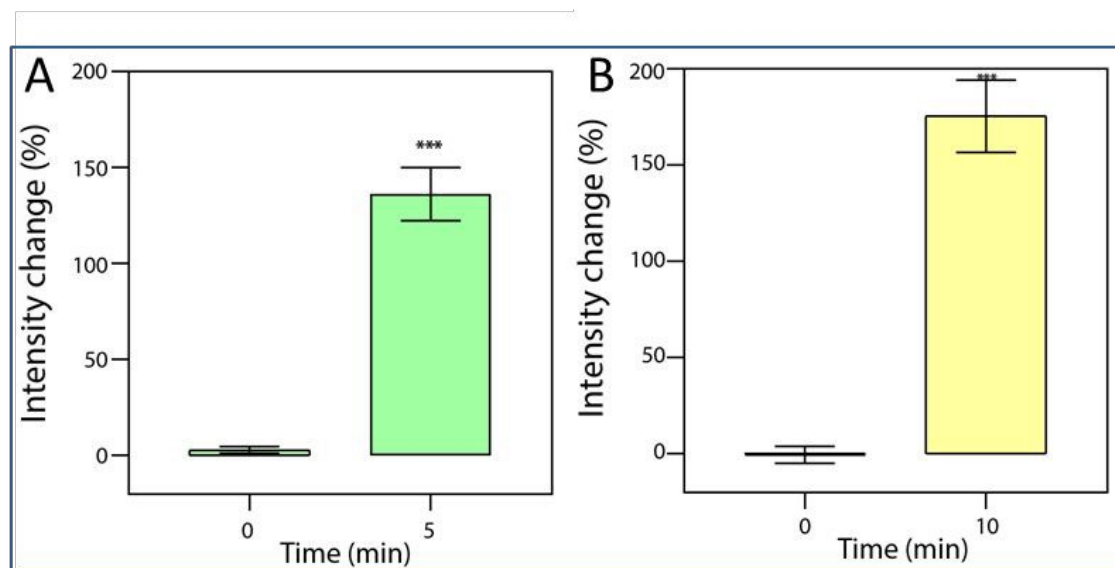


Fig 9: Remarkable increase in the fluorescent intensity of probes with progressive excitation: A) C-1 Average intensity of individual lipid droplets at 0 mins and 10 min. B) J-1: Average intensity of individual lipid droplets at 0 mins and 5 min. $n = 65$; *** $P < 0.0001$ (Paired t -test).

Both J-1 and C-1 showed potent application in staining lipid droplets inside the cell. However, for any probe to be effectively used for bio-applications, their effect on the cell viability is an important parameter. To check the effect of these probes on cell viability, we performed an MTT assay across a wide range of concentrations, ranging from 100 nM to 1000 nM. Our results indicated that while C-1 was toxic at higher concentrations (Figure- 10A), J-1 was not cytotoxic even after 24 h of treatment (Fig. 10B).

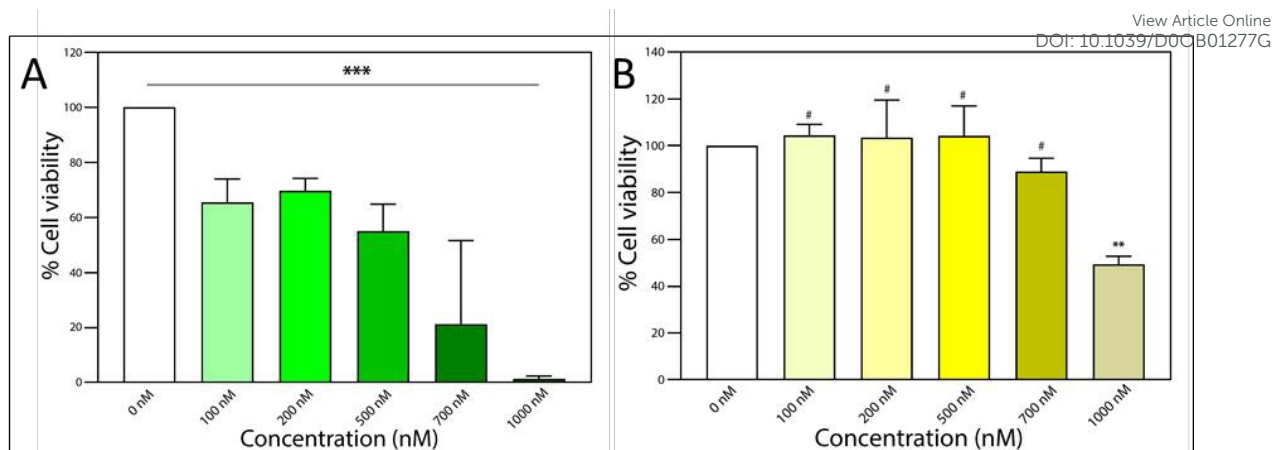


Fig. 10: Cell viability assays. A) C-1 and B) J-1. HeLa cells incubated with varying concentrations of the probes for 24 h were used for the MTT assay. The values are represented as mean \pm SD ($n=3$; #: not significant; ** $P < 0.01$ (Student t -test); *** $P < 0.0001$ (ANOVA)).

Conclusions

In this work, styryl derivatives containing coumarin and pyridine scaffolds were designed and synthesised. The fluorophores show significant Stokes shift with emission > 550 nm. Live-cell imaging experiments demonstrate selective staining of the lipid droplets at lower concentrations of the fluorophores with a high signal-to-noise ratio at low concentrations. The fluorophores also show strong biocompatibility and excellent photostability. This work provides a simpler way to visualize the lipid droplets and provide powerful tools to unravel the dynamics of lipid droplets.

Supporting Information

Comparative T=Table of recently published literature (Table S1), ^1H and ^{13}C NMR data and lipid droplet localization videos.

Acknowledgments

A financial grant from the SERB (CRG/2018/004020) is appreciated. VS, AS acknowledge DBT (Grant No.: BT/PR15214/BRB/10/1449/2015 and BT/RLF/Re-entry/45/2015) and DST-SERB (Grant No.: ECR/2016/000913) for financial support. PJ acknowledges a fellowship from IIT Gandhinagar. We also thank reviewers for the insightful suggestions.

References

View Article Online
DOI: 10.1039/D0OB01277G

1. A. R. Thiam and M. Beller, *J. Cell Sci.*, 2017, **130**, 315-324.
2. M. Beckman, *Science*, 2006, **311**, 1232.
3. D. J. Murphy, *Prog. Lipid Res.*, 2001, **40**, 325-438.
4. Y. Miyanari, K. Atsuzawa, N. Usuda, K. Watashi, T. Hishiki, M. Zayas, R. Bartenschlager, T. Wakita, M. Hijikata and K. Shimotohno, *Nature Cell Biol.*, 2007, **9**, 1089-1097.
5. A. R. Thiam, R. V. Farese Jr and T. C. Walther, *Nature Rev. Mol. Cell Biol.*, 2013, **14**, 775.
6. N. A. Ducharme and P. E. Bickel, *Endocrinology*, 2008, **149**, 942-949.
7. D. L. Brasaemle, *J. Lipid Res.* 2007, **48**, 2547-2559.
8. Y. Guo, K. R. Cordes, R. V. Farese and T. C. Walther, *J Cell Sci*, 2009, **122**, 749-752.
9. M. A. Welte and A. P. Gould, *Biochim. Biophys. Acta -Mol. Cell Biol. Lipids*, 2017, **1862**, 1260-1272.
10. H. L. Ploegh, *Nature*, 2007, **448**, 435.
11. H. A. Saka and R. Valdivia, *Ann. Rev. Cell Developmental Biol.*, 2012, **28**, 411-437.
12. M. A. Welte, *Current Biology*, 2015, **25**, R470-R481.
13. A. D. Barbosa, D. B. Savage and S. Siniossoglou, *Curr. Opin. Cell Biol.* 2015, **35**, 91-97.
14. T. C. Walther and R. V. Farese Jr, *Ann. Rev. Biochem.*, 2012, **81**, 687-714.
15. G. Onal, O. Kutlu, D. Gozuacik and S. D. Emre, *Lipids in health and disease*, 2017, **16**, 128.
16. T. K. Fam, A. S. Klymchenko and M. Collot, *Materials*, 2018, **11**, 1768.
17. M. Collot, T. K. Fam, P. Ashokkumar, O. Faklaris, T. Galli, L. Danglot and A. S. Klymchenko, *J. Am. Chem. Soc.*, 2018, **140**, 5401-5411.
18. L. L. Listenberger and D. A. Brown, *Curr. Protocols Cell Biol.*, 2007, **35**, 24.22.21-24.22.11.
19. K. Kikuchi, *Chem. Soc. Rev.*, 2010, **39**, 2048-2053.
20. A. H. Ashoka, P. Ashokkumar, Y. P. Kovtun and A. S. Klymchenko, *J. Phys. Chem. Lett.*, 2019.
21. O. Darragh, A. Byrne, G. B. Berselli, C. Long and T. E. Keyes, *Analyst*, 2019, **144**, 1608-1621.
22. J.-B. Li, H.-W. Liu, T. Fu, R. Wang, X.-B. Zhang and W. Tan, *Trends Chem.*, 2019, **1**, 224-234.
23. P. Greenspan, E. P. Mayer and S. D. Fowler, *J. Cell Biol.* 1985, **100**, 965.
24. J. Spandl, D. J. White, J. Peychl and C. Thiele, *Traffic*, 2009, **10**, 1579-1584.
25. A. Tabero, F. García-Garrido, A. Prieto-Castañeda, E. Palao, A. R. Agarrabeitia, I. García-Moreno, A. Villanueva, S. de la Moya and M. J. Ortiz, *Chem. Comm.*, 2020, **56**, 940-943.
26. J. H. Lee, J.-H. So, J. H. Jeon, E. B. Choi, Y.-R. Lee, Y.-T. Chang, C.-H. Kim, M. A. Bae and J. H. Ahn, *Chem. Comm.*, 2011, **47**, 7500-7502.
27. Y. Li, M. Zhang, X. Chen, J. Liang, D. Chen, M. Gao and L. Ren, *Tet. Lett.*, 2019, **60**, 1880-1884.
28. M. Collot, S. Bou, T. K. Fam, L. Richert, Y. Mély, L. Danglot and A. S. Klymchenko, *Anal. Chem.*, 2019, **91**, 1928-1935.
29. R. Matsubara, T. Kaiba, A. Nakata, T. Yabuta, M. Hayashi, M. Tsubaki, T. Uchino and E. Chatani, *J. Org. Chem.*, 2019, **84**, 5535-5547.
30. S. I. Suarez, C. C. Warner, H. Brown-Harding, A. M. Thooft, B. VanVeller and J. C. Lukesh, *Org. Biomol. Chem.*, 2020, **18**, 495-499.
31. J. Zheng, S. Feng, S. Gong, Q. Xia and G. Feng, *Sens. Act. B: Chem.*, 2020, **309**, 127796.
32. F. Yu, X. Jing and W. Lin, *Sens. Act. B Chem.*, 2020, **302**, 127207.
33. Y. Chen, X.-R. Wei, R. Sun, Y.-J. Xu and J.-F. Ge, *Org. Biomol. Chem.*, 2018, **16**, 7619-7625.
34. X.-Z. Yang, R. Sun, X. Guo, X.-R. Wei, J. Gao, Y.-J. Xu and J.-F. Ge, *Dyes Pigments.*, 2020, **173**, 107878.
35. P. Jana, M. Radhakrishna, S. Khatua and S. Kanvah, *Phys. Chem. Chem. Phys.*, 2018, **20**, 13263-13270.
36. P. Jana, N. Patel, V. Soppina and S. Kanvah, *New J. Chem.*, 2019, **43**, 584-592.
37. D. Cao, Z. Liu, P. Verwilt, S. Koo, P. Jangjili, J. S. Kim and W. Lin, *Chem. Rev.*, 2019, **119**, 10403-10519.
38. A. Gandioso, R. Bresolí-Obach, A. Nin-Hill, M. Bosch, M. Palau, A. Galindo, S. Contreras, A. Rovira, C. Rovira, S. Nonell and V. Marchán, *J. Org. Chem.*, 2018, **83**, 1185-1195.

39. W. Wang, X.-J. Han, J.-T. Liu, J.-Y. Miao and B.-X. Zhao, *Dyes Pigm.*, 2020, **173**, 107892. [View Article Online](#)
DOI: 10.1039/D0OB01277G
40. X. Pei, H. Tian, W. Zhang, A. M. Brouwer and J. Qian, *Analyst*, 2014, **139**, 5290-5296.
41. B.-K. An, J. Gierschner and S. Y. Park, *Acc. Chem. Res.*, 2012, **45**, 544-554.
42. B. Xu, J. He, Y. Dong, F. Chen, W. Yu and W. Tian, *Chem. Comm.* 2011, **47**, 6602-6604.
43. C. W. Song, U. Tamima, Y. J. Reo, M. Dai, S. Sarkar and K. H. Ahn, *Dyes Pigm.*, 2019, **171**, 107718.
44. C.-C. Wang, S.-Y. Yan, Y.-Q. Chen, Y.-M. Zhou, C. Zhong, P. Guo, R. Huang, X.-C. Weng and X. Zhou, *Chinese Chem. Lett.*, 2015, **26**, 323-328.
45. R. V. Farese Jr and T. C. Walther, *Cell*, 2009, **139**, 855-860.
46. M. Kumar, S. Ojha, P. Rai, A. Joshi, S. S. Kamat and R. Mallik, *J. Cell Biol.*, 2019, **218**, 3697-3713.
47. A. Kassan, A. Herms, A. Fernández-Vidal, M. Bosch, N. L. Schieber, B. J. N. Reddy, A. Fajardo, M. Gelabert-Baldrich, F. Tebar and C. Enrich, *J Cell Biol*, 2013, **203**, 985-1001.
48. H. Varinli, M. J. Osmond-McLeod, P. L. Molloy and P. Vallotton, *J. Lipid Res.*, 2015, **56**, 2206-2216.
49. S. Missaglia, R. A. Coleman, A. Mordente and D. Tavian, *Cells*, 2019, **8**, 187.
50. R. F. Schwabe and J. J. Maher, *Gastroenterology*, 2012, **142**, 8.
51. S. Murphy, S. Martin and R. G. Parton, *PLoS one*, 2010, **5**, e15030.